Supporting Information

Microstructure in as-implanted crystals

The damaged layers in the as-implanted crystal wafers are the regions containing the injected ions, which are up to 40 nm deep as suggested from the SRIM (the Stop and Range of Ions in Matter) simulation. The damage present within the damaged layers can be different at different depth. In the as-implanted crystals with 0.2 at.% Pr (and 2 at.% Al), we observed a 30-40 nm thick damaged layer with heavy damage occurring in the range of 15-30 nm depth from the surfaces. As shown in the HAADF images **fig.S1**(**a**), the damaged layers contain bright crystalline nano-domains distributed in the dark background. In the as-implanted crystals with 2.8 at.% Pr (see **fig.S1**(**b**)), a ~25-30 nm thick amorphous or near amorphous layer (e.g. the region with comparable dark contrast in HAADF images) and 7-15 nm thick mosaic layer with small mis-orientated crystalline domains are recorded.

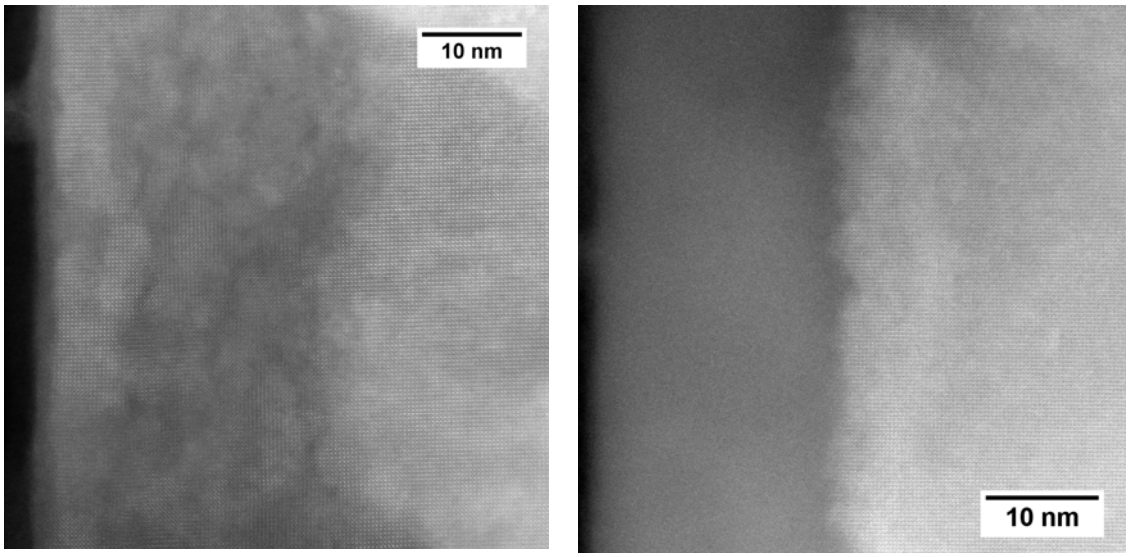

(a) 0.2 at.% Pr and 2 at.% Al (b) 2.8 at.% Pr

Figure S1. STEM-HAADF images of as-implanted $SrTiO_3$ single crystals. The ions were injected from left to right into the bulk

Dislocations present at the implantation front:

Under STEM mode, the standard bright field images cover a region of the Ronchigram, the central zero-order disc of the convergent beam electron diffraction pattern. Similar to BF images under TEM mode, the STEM-BF images are dominated by the diffraction contrast, which is sensitive to the change of periodic structure of a lattice. Thus, dislocations caused by the disorder of the lattice are clearly visible from the BF images. In the fully recrystallized samples, dislocations are mainly distributed at the implantation front as demonstrated in **fig.S2**(**b**). These dislocations appear with bright butterfly-shape contrast in modified ABF images. In addition, the nanoclusters shown in HAADF images do not have corresponding contrast in the BF images suggesting their different contrast mechanisms.

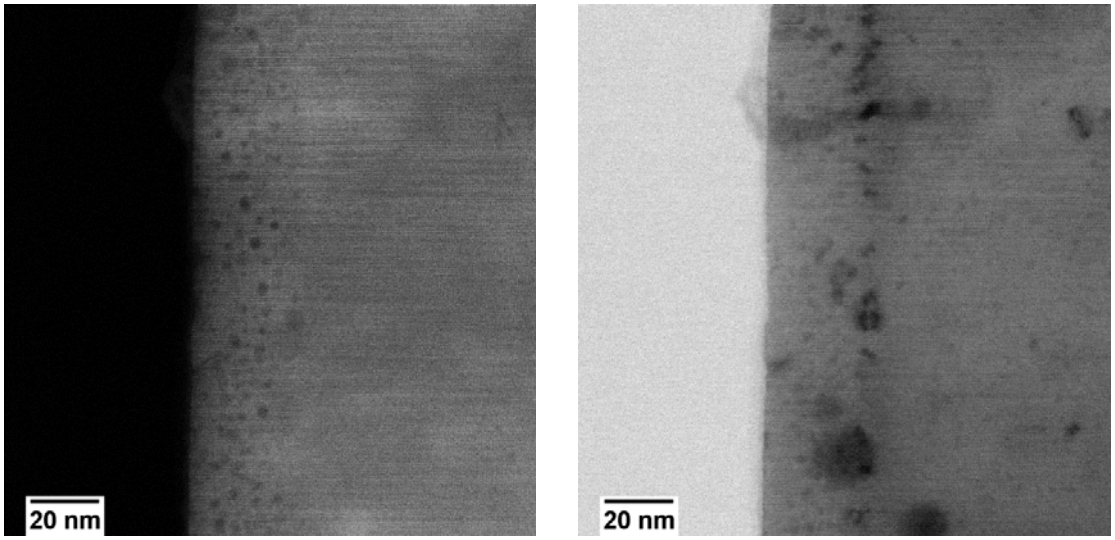

(a) HAADF (b) BF

Figure S2. Dislocations at the implantation front

Microstructure in the sample with 90˚ rotation

The appearance and the shape of dark-contrast nano-clusters are additionally confirmed by the same morphology detected in a sample prepared with 90˚ rotation with respect to the one in **fig. 2**.

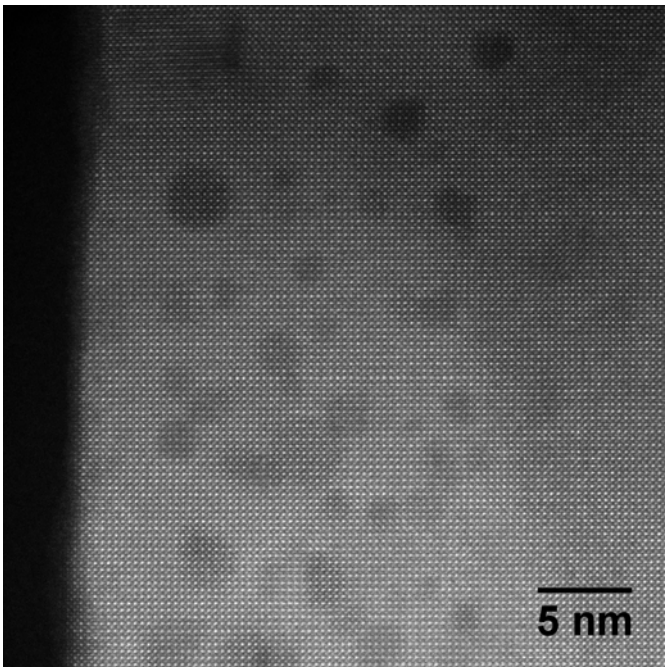

Figure S3 STEM-HAADF images of a annealed sample with 0.2 at.% Pr and 2 at.% Al.

EELS map of Pr dopants

In order to further support our conclusion of Pr dopants, another EELS map of Pr dopants is presented here. Pr dopants are randomly distributed at some of the Sr-sites. Within the similar area in **fig.1**, approximately five Pr dopants are recorded as shown in **fig.S4**. These facts are consistent with the results presented in **fig.1**. About ten other similar maps show comparable results.

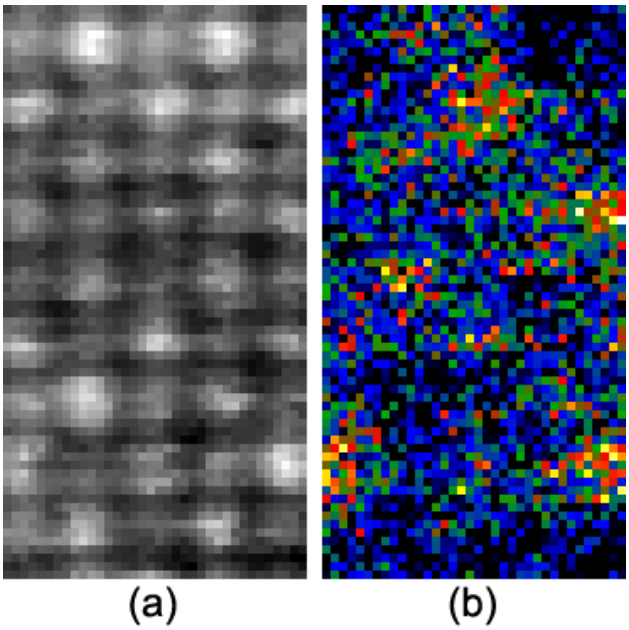

Figure S4. EELS map of Pr dopants within the same specimen in **fig.1**. (a) the HAADF images acquired simultaneously with an EEL spectrum images; (b) the chemical map of Pr dopants extracted from the raw dataset.

The visibility tests of Pr:

Here we include calculations of larger Pr-clusters or detection of the single Pr atom profiles supporting the conclusion on clusters and thickness. The simulation code was implemented by Kirkland[19] based on the multislice approach and frozen phonon model to account for the effect of thermal vibration of the lattice. In order to reduce the interaction between adjacent dopants, the target dopant(s) was isolated in a large periodic unit cell 27.335 Å x 27.335 Å x t, in which t is the local thickness up to 50.8Å. Simulation codes also take into account of experimental convergence angle of the probe, aberrations of the lens, as well as collection angle of the detector.

Fig. S5 demonstrates the visibility of single Pr atom based on a simple assumption that a single Pr ion occupies a Sr-lattice site. As shown in the insert in **fig. S5** (**b**), I_{Pr} and I_{Sr} are defined as the intensities at Pr-occupied positions and Sr-lattice sites, respectively. The visibility of single Pr atom is indicated as the intensity ratio between the Pr-occupied lattice site and the normal lattice site. The intensity of the Pr-occupied lattice site I_{Pr} varies with the position of the Pr within the atomic column, as shown in **fig.S5**(**a**). The fine scale fluctuation may be caused by computation artifacts such as thickness sampling within the multislice simulations. The most visible depth of Pr atom is approximately 2-3 nm from the entrance surface of the sample. At the optimal position of the Pr dopant, the Pr dopants are hardly visualized when the thickness of the sample is larger than 2 nm, as shown in **fig.S5**(**b**).

In **fig.S6**(**a**), a Pr-occupied lattice site is barely visible within a sample with the thickness of 2.3 nm. However, under the same observation conditions, Pr ions are more easily observed as bright dots in the simulated HAADF images when forming a cluster, as shown in **fig.S6**(**b**).

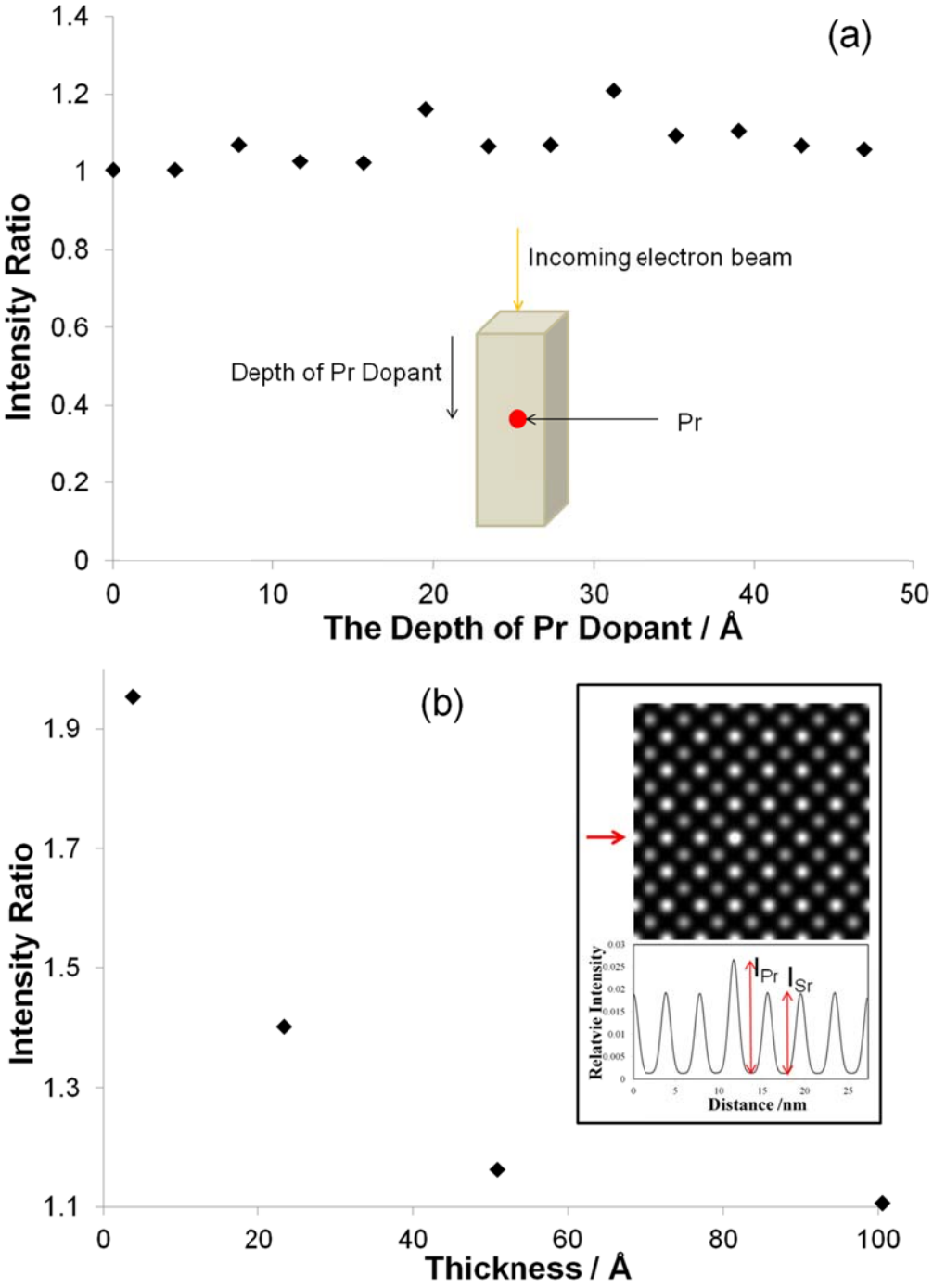

Figure S5 The detectability of Pr sitting in a substitutional position of Sr or Ti. The intensity ratio is defined from the line scanning profile contain the Pr atoms within the lattice. The super unit cell used in (a) is 27.335 Å x 27.335 Å x 50.8 Å.

(a) single Pr (b) Pr_8

Figure S6 The detectability of Pr clusters.

Pure Nano-cluster EEL spectrum

Due to the fact that these nano-clusters immerged into the bulk lattice, signals contributed by these nano-clusters cannot be physically separated from the bulk signals. However, EEL spectra for different components, i.e., a nano-cluster and the bulk, can be isolated through a series of EELS measurement and their known contribution ratios[26]. Since the EEL spectra is acquired for a very thin specimen (t ~7 nm thick, within a single scattering regime), the EELS signals (E_{mix}, 1xn matrix, n is the number of energy channels) from a nano-cluster and the bulk are integrated linearly as the incident beam passes through the specimen. Therefore, the contribution by a nano-cluster ($t_{nano\text{-}cluster}/t$) can be estimated from its dimension $t_{nano\text{-}cluster}$ and the local thickness t.

A bulk EEL spectrum ($E_{bulk,}$ 1xn matrix, n is the number of energy channels) acquired from the surrounding region without nano-clusters is normalized with respect to E_{mix} according to the contimuum past the edge (above 15 eV) to remove the possible instability of the electron beam. Therefore, the EEL spectrum from a nano-cluster is numerically separated from E_{mix} by subtracting the bulk contribution, which is estimated from E_{bulk} plus its contributions (1- $t_{nano\text{-}cluster}/t$).